Article

Current Biology

Pluripotent Pericycle Cells Trigger Different Growth Outputs by Integrating Developmental Cues into Distinct Regulatory Modules

Highlights

- Auxin is required for phellogen establishment and maintenance
- Lateral root formation is the main auxin-induced program after plant greening
- The establishment of the vascular cambium is required for periderm initiation
- Different targets downstream of auxin control lateral root and periderm formation

Authors

Wei Xiao, David Molina, Anna Wunderling, Dagmar Ripper, Joop E.M. Vermeer, Laura Ragni

Correspondence

laura.ragni@zmbp.uni-tuebingen.de

In Brief

Xiao et al. describe how root pericycle output specificity is achieved. Auxin promotes LR and periderm formation through distinct transcription factors and via the integration of developmental cues.

Xiao et al., 2020, Current Biology *30*, 4384–4398
November 16, 2020
https://doi.org/10.1016/j.cub.2020.08.053

CellPress

CellPress

Current Biology

Article

Pluripotent Pericycle Cells Trigger Different Growth Outputs by Integrating Developmental Cues into Distinct Regulatory Modules

Wei Xiao,[1] David Molina,[1,3] Anna Wunderling,[1,3] Dagmar Ripper,[1] Joop E.M. Vermeer,[2] and Laura Ragni[1,4,*]
[1]ZMBP-Center for Plant Molecular Biology, University of Tübingen, Auf der Morgenstelle 32, 72076 Tübingen, Germany
[2]Institute of Biology, University of Neuchâtel, Rue Emile-Argand 11, 2000 Neuchâtel, Switzerland
[3]These authors contributed equally
[4]Lead Contact
*Correspondence: laura.ragni@zmbp.uni-tuebingen.de
https://doi.org/10.1016/j.cub.2020.08.053

SUMMARY

During post-embryonic development, the pericycle specifies the stem cells that give rise to both lateral roots (LRs) and the periderm, a suberized barrier that protects the plant against biotic and abiotic stresses. Comparable auxin-mediated signaling hubs regulate meristem establishment in many developmental contexts; however, it is unknown how specific outputs are achieved. Using the *Arabidopsis* root as a model, we show that while LR formation is the main auxin-induced program after de-etiolation, plants with age become competent to form a periderm in response to auxin. The establishment of the vascular cambium acts as the developmental switch required to trigger auxin-mediated periderm initiation. Moreover, distinct auxin signaling components and targets control LR versus periderm formation. Among the periderm-specific-promoting transcription factors, *WUSCHEL-RELATED HOMEOBOX 4* (*WOX4*) and *KNAT1/BREVIPEDICELLUS* (*BP*) stand out as their specific overexpression in the periderm results in an increased number of periderm layers, a trait of agronomical importance in breeding programs targeting stress tolerance. These findings reveal that specificity in pericycle stem cell fate is achieved by the integration of developmental cues into distinct regulatory modules.

INTRODUCTION

The plant body consists of developmental units that are constantly produced by the stem cells located at the meristems. Primary meristems, such as the shoot and the root apical meristems, are formed during embryogenesis, while secondary meristems arise from differentiated cells or a mixture of differentiated and undifferentiated tissues that reacquire pluripotency during plant growth. Examples of secondary meristems are the vascular cambium and the phellogen/cork cambium, which are responsible for the increase in the girth of plant organs [1]. Both meristems divide bidirectionally, producing inward wood and phelloderm and outward phloem and phellem/cork, respectively [1, 2] (Figure 1A). While the vascular cambium in trees remains active throughout a tree's life, the phellogen may be replaced every year or after several years from the tissue underneath [3]. The phellogen, the phelloderm, and the phellem are usually referred to as the periderm. Phellem cells are highly suberized and lignified and act as a barrier, which restricts gas exchange, water loss, and pathogen attack [1, 3–5]. In most plant species, the stem phellogen originates from the subepidermal layer, whereas in roots, including *Arabidopsis*, root phellogen arises from the pericycle, an inner tissue that is surrounded by several cell layers (endodermis, cortex, and epidermis). If the first phellogen is superficial (as in stems), then only small amounts of primary tissues are shed during periderm growth, whereas deeper periderms slough away large amounts of primary tissues (as in roots). In the *Arabidopsis* root, periderm development can be dissected in 5 distinct stages in connection with the fate of the tissues surrounding the pericycle (Figures 1A and S1A).

Briefly, at stage 1, the pericycle cells located at the xylem poles start to proliferate, and then anticlinal cell divisions extend to the whole pericycle [3, 6]. At stage 2, the pericycle divides also periclinally, forming the meristematic ring comprising the phellogen, whereas the endodermis undergoes programmed cell death (PCD) [3, 6]. During stages 3 to 5, cork cells differentiate, and the epidermis and the cortex are sloughed away [3, 6]. Lateral roots (LRs), and to a lesser extent, the vascular cambium, also arise from xylem pole pericycle cells, highlighting the unique pluripotency capacity of this tissue [7, 8]. An auxin maxima specifies LRs in the region above the root apical meristem, and the first formative divisions occur before the onset of secondary growth; thus, LR formation precedes periderm initiation [9]. During LR emergence, similar to periderm development, the endodermis loses volume and can undergo PCD, whereas the epidermis and the cortex are pushed away to accommodate primordia outgrowth [10, 11].

It is known that conserved regulatory networks, including those triggered by auxin, play a major role in stem cell establishment and maintenance in the embryo, shoot and root apical

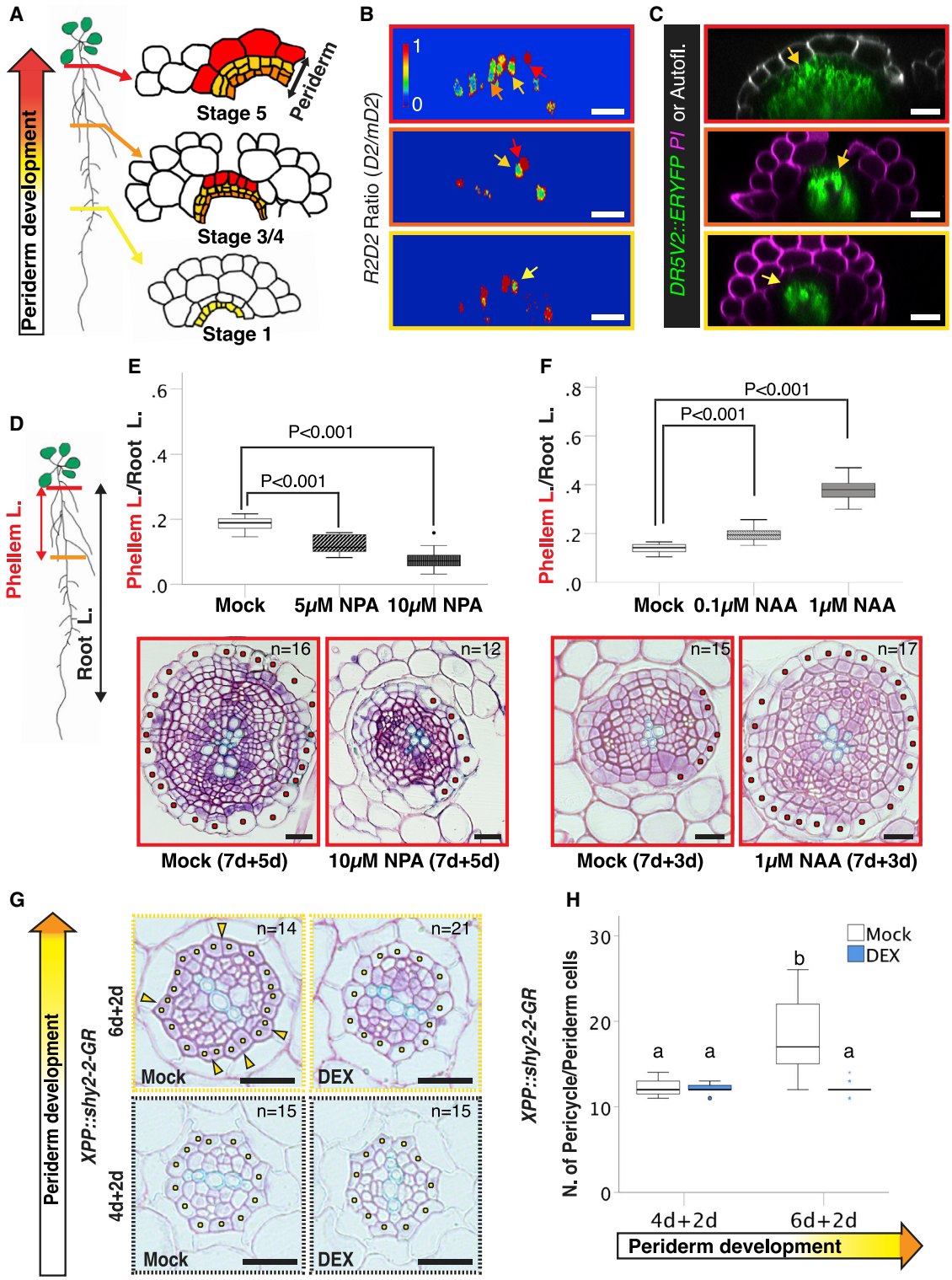

Figure 1. Auxin Promotes Phellogen Establishment from the Pericycle

(A) Periderm development in the *Arabidopsis* root can be followed along the root. Schematic of periderm development stages (pale yellow: pericycle; orange: phelloderm, dark yellow: phellogen, and red: phellem).

(B) Ratio of the relative intensities of D2-Venus/mD2-dTomato of the pictures shown in Figure S1B.

(C) Orthogonal view of z stacks of a *DR5v2::ER-YFP* root at the positions corresponding to stage 1 (bottom), stage 3/4 (center), and stage 5 (top) (12 days old).

(legend continued on next page)

meristems, and the vascular cambium [12, 13]. Specific auxin-mediated signaling modules are active in different organs/tissues [8, 12, 14–17]; however, our understanding about how tissue output specificity is achieved is limited. Here, we investigated how two independent developmental programs, LR and periderm formation, are initiated from the same tissue.

RESULTS

Auxin Is Required for Periderm Establishment from the Pericycle

As the regulatory networks underlying periderm formation are largely unknown, we assessed whether auxin plays a role during phellogen establishment. Periderm development can be followed over space along the same root (which represents a developmental gradient) or over time in the same zone of the root (e.g., the most mature close to the hypocotyl) (Figures 1A and S1A) [6]. We mapped auxin distribution and activity at 3 representative stages of periderm formation, exploiting the genetically encoded biosensors *R2D2* and *DR5v2* [18]. *R2D2* is based on the auxin-induced degradation of a fluorophore (*RPS5A::D2-Venus*) coupled to a nondegradable internal control (*RPS5A::m-dTomato*). Hence, the ratio between the 2 fluorescent signals reports auxin cellular concentrations. We found that auxin accumulates in the xylem pole pericycle cells during periderm initiation (stage 1) and in the phellogen during periderm development (stage 3/4) (Figures 1B, S1B, and S1C). In a mature periderm, auxin levels peak in both phellogen and phelloderm. Consistently, an auxin minimum was detected in phellem cells (Figures 1B, S1B, and S1C). In line with this, auxin activity, as shown by *DR5v2::ER-YFP*, is high in the phellogen and phelloderm and low in the phellem (stages 3/4 and 5) (Figure 1C). Next, we blocked polar auxin transport by treating plants (7 days old), initiating periderm formation with N-1-naphthylphthalamic acid (NPA) for 5 days. In mock-treated plants, ¼ of the root (~2.5 cm), was covered by the phellem, whereas in NPA-treated plants, both phellem length and phellem ratio were significantly reduced (Figures 1D, 1E, and S1D). In addition, phellem (red dots) differentiation was incomplete in NPA-treated roots, indicating a delay in periderm development (Figure 1E). By contrast, treatment with auxin (1-Naphthaleneacetic acid [NAA], Indole-3-acetic acid [IAA], or 2,4-Dichlorophenoxyacetic acid [2,4-D]) promoted periderm formation as shown by an increased phellem length and phellem ratio (Figures 1F and S1E–S1G). Moreover, in cross-sections of NAA-treated plants, we observed that phellem cells were already differentiated and covered the whole root, whereas in the mock control, only a few phellem cells were present (Figure 1F). These results highlight the importance of auxin for periderm growth and initiation.

To further dissect the role of auxin during periderm development, we engineered plants to specifically block auxin signaling in the pericycle at the onset of periderm formation and in the phellogen at periderm maturity. This was achieved by using spatial and temporal controlled expression of stabilized Aux/IAA variants [19]. The *XYLEM POLE PERICYCLE* (*XPP*) promoter is active at the onset of periderm initiation in the xylem pole pericycle cells [20], whereas the *PEROXIDASE15* (*PER15*) promoter is expressed in the whole pericycle at stage 1 and in both phellem and phellogen at stage 5 of periderm development (Figures S1H and S1I). We observed that prolonged induction of *XPP::shy2-2-GR* and *PER15::slr-1-GR* (7–12 days) resulted in reduced phellem length, phellem ratio, and disorganized periderm (Figures S2A and S2B). Consistently, hindering the transcriptional auxin response precisely at the onset of periderm development abolished cell divisions in the pericycle and the expression of the periderm marker *MYB84* [6] (Figures 1G, 1H, and S2C–S2E), indicating that auxin signaling is required to trigger periderm initiation. Next, we investigated whether auxin is necessary to maintain stem cell activity in the phellogen, by inducing the *PER15::slr-1-GR* construct in a fully differentiated periderm (12 days old) (Figure S2F). A prolonged dexamethasone (DEX) induction (8 days) resulted in the loss of phellogen activity and *MYB84* expression (Figure S2F). As expected, cork cells were still suberized (Figure S2G), showing that stem cell activity can be stopped but cells cannot dedifferentiate. In summary, our results demonstrate that auxin-mediated transcriptional reprogramming is required for periderm establishment and development. Thus, auxin promotes both LR and periderm programs from the pericycle, raising the question of how auxin output specificity is achieved.

LR Formation Is the Main Auxin-Induced Program in the Pericycle after Plant Greening, whereas Plants with Aging Become Competent to Respond to Auxin to Form the Periderm

To investigate auxin specificity, we tested whether the dynamics of auxin responses differ during LR and periderm development. We studied the effect of a short auxin treatment (48 h) in plants before (4 day old), at (6 day old), and after the onset of periderm formation (8 day old) [6]. Auxin treatment resulted in roots with an

(D) Schematic representation of an *Arabidopsis* root showing how phellem length (phellem L. [cm]) and phellem ratio (phellem length [cm]/root length [cm]) are measured.

(E) Top: quantification of phellem length in 12-day-old WT roots. Seven-day-old plants were treated for 5 days with mock, 5 μM NPA, or 10 μM NPA; t test (n = 15). Lower panels: cross-sections (plastic embedding) of the uppermost part of 12-day-old WT roots. Seven-day-old plants were transferred for 5 days to mock or 10 μM NPA plates.

(F) Top: quantification of phellem ratio in 10-day-old WT roots. Seven-day-old plants were transferred to mock, 0.1 μM, or 1 μM NAA plates for 3 days; t test (n = 15). Bottom: cross-sections (plastic embedding) of the uppermost part of 10-day-old WT roots. Seven-day-old plants were transferred to mock or 1 μM NAA plates for 3 days.

(G) Cross-sections (plastic embedding) of the uppermost part of *XPP::shy2-2-GR* (in *MYB84::NLS-3xGFP W131Y;#1*) roots. Four- and 6-day-old plants were treated for 2 days with mock or 10 μM DEX.

(H) Quantification of number of pericycle/periderm cells of (G). One-way ANOVA (95% confidence interval [CI], post hoc: Tamhane, n = 15–21).

The pale yellow arrows indicate the pericycle, the dark yellow arrows indicate the phellogen, the red arrows indicate the phellem, and the orange arrows indicate the phelloderm. The red dots represent the phellem cells and the yellow dots represent the pericycle cells. Black and white scale bars: 20 μm.

See also Figures S1 and S2 and Data S2.

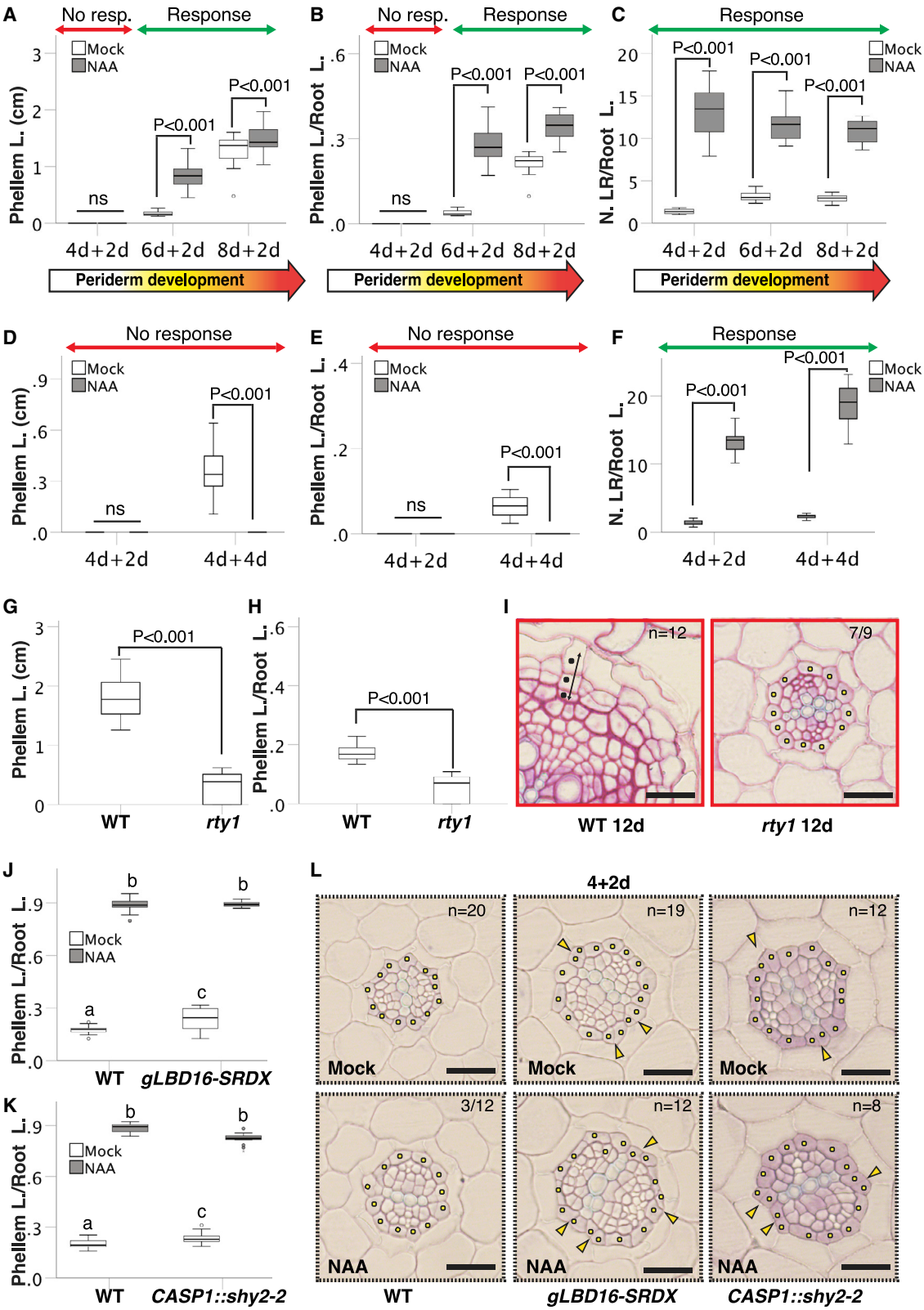

Figure 2. Auxin Is Not Sufficient to Induce Periderm Formation

(A and B) Quantification of phellem length (A) and phellem ratio (B) in WT (*MYB84::NLS-3xGFP W131Y*) roots. Four-, 6-, and 8-day-old plants were treated for 48 h with mock or 1 μM NAA; t test (ns, not significant; n = 14–15).

(legend continued on next page)

increased phellem length and phellem ratio only when plants were treated upon periderm initiation time or later (Figures 2A and 2B). In contrast, auxin induced LR formation independent of the plant developmental stage after the body of the plant is established (after de-etiolation/greening occurred: hypocotyl has stopped elongation and the cotyledons are opened) (Figures 2C and S3A–S3C). Consistently, the periderm marker *MYB84* [6] is not expressed in 4-day-old auxin-treated plants, indicating that the periderm program is not triggered (Figure S3D). In line with this, we observed that a 20-h auxin treatment was sufficient to increase the number of pericycle divisions (quantified using the microtubule marker *35S::GFP-TUA6* [21]) at the onset of periderm formation (6-day-old plants) but not before (Figures S3E and S3F). Auxin did not induce periderm formation in 4-day-old plants, even when auxin treatment was prolonged to 4 days (Figures 2D and 2E). These plants kept producing LRs and no periderm was initiated, while mock roots had already started the periderm program (Figures 2F and S3G), pointing out that plants with age become competent to establish periderm in response to auxin.

To corroborate our results, we investigated periderm development in the auxin-overproducing mutant *superroot1/rooty1*(*rty1-1*) [22, 23]. In line with our auxin-feeding experiments, in *rty1* mutants periderm growth was almost blocked as seen by a drastic reduction in phellem length and phellem ratio and by the absence of pericycle divisions in the majority of the observed roots (Figures 2G–2I). These results suggest that LR formation is the main developmental program activated by auxin in the pericycle (after greening), and that periderm initiation requires the integration of additional developmental cues.

Blocking LR Initiation Has a Positive Effect on Periderm Growth

We next asked whether blocking LR formation in the zone of the root where periderm initiation occurs acts as a trigger for the periderm program. Thus, we quantified periderm growth in 2 independent genetic backgrounds, which lack LRs without altering auxin signaling in the periderm. In *CASP1::shy2-2* plants, LR initiation is arrested by blocking auxin signaling in the endodermis, whereas in *gLBD16-SRDX* lines, LATERAL ORGAN BOUNDARIES-DOMAIN 16 (LBD16), a transcription factor (TF) that acts downstream of auxin to promote LRs, is turned into a repressor [10, 24–26]. In both lines, we observed a mild increase in phellem length and phellem ratio when compared to wild type (WT), whereas upon auxin induction (7 days + 5 days), they were indistinguishable from WT, suggesting that the lack of LRs induces early periderm onset (Figures 2J, 2K, S3H, and S3I). To confirm it, we quantified the number of pericycle cells at the onset of periderm formation. In 6-day-old roots, the pericycle cell number was higher in both *CASP1::shy2-2* and *gLBD16-SRDX* compared to WT, and the effect was larger in 8-day-old plants (Figures 2L and S3K–S3M). However, the absence of LRs did not confer early competence to auxin to form a periderm, indicating that precocious periderm initiation in these lines may be indirectly triggered by other factors (Figures 2L and S3K-S3M). Supporting this, the number of vascular cells was also increased in *CASP1::shy2-2* and *gLBD16-SRDX* roots (Figure S3N).

The Establishment of the Vascular Cambium Acts as the Developmental Switch That Triggers the Auxin-Mediated Periderm Program

We noticed that in *CASP1::shy2-2* and *gLBD16-SRDX,* the establishment of the vascular cambium occurs earlier (Figure S3N), while in *rty1* mutants it is delayed (Figure 2I). We hypothesized that the formation of the vascular cambium may act as the developmental switch that is required to elicit periderm formation. In support of this hypothesis, a periderm is present only in species that undergo massive secondary growth [3, 4]. The onset of periderm development follows the first divisions in the pro-cambium, and the 2 meristems appear to develop simultaneously (Figure S4A). To validate this experimentally, we tested the effect of impaired cambium activity on periderm development. Loss of function of the master regulator of cambial activity *PHLOEM INTERCALATED WITH XYLEM/ TDIF RECEPTOR* (*PXY/TDR),* which is not expressed in the periderm (Figure S4B), results in altered cambium patterning and decreased cambium proliferation [27, 28]; thus, we inspected *pxy-3* mutants for periderm phenotypes. At 8 days, the whole pericycle is dividing in WT plants and the first periclinal divisions have already occurred, whereas in *pxy* mutants only a few divisions took place (Figures 3A and 3B). Moreover, phellem length, phellem ratio, and the periderm auxin response were highly reduced in *pxy* mutants (Figures 3C and S4C), suggesting that the vascular cambium is necessary for periderm formation. To further substantiate these findings, we exploited the fact that blocking auxin-mediated transcriptional responses in the *PXY* expression domain arrests cambium activity [14] without altering

(C) Quantification of LR density of WT (*MYB84::NLS-3xGFP W131Y*) roots. Four-, 6-, and 8-day-old plants were treated for 48 h with mock or 1 μM NAA; t test (n = 14–15).
(D–F) Quantification of phellem length (D), phellem ratio (E), and lateral root density (F) in WT roots. Four-day-old plants were treated for 96 h with mock or 1 μM NAA; t test (ns: not significant, n = 15).
(G and H) Quantification of phellem length (G) and phellem ratio (H) in 12-day-old WT and *rty* roots; t test (n = 15).
(I) Cross-sections (plastic embedding) of the uppermost part of 12-day-old WT and *rty1* roots.
(J) Quantification of phellem ratio in 12-day-old WT and *gLBD16-SRDX* roots. Seven-day-old plants were treated for 5 days with mock or 1 μM NAA. One-way ANOVA (95% CI, post hoc: Tamhane, n = 15).
(K) Quantification of phellem ratio in 12-day-old WT and *CASP1::shy2-2* roots. Seven-day-old plants were treated for 5 days with mock or 1 μM NAA. One-way ANOVA (95% CI, post hoc: Bonferroni, n = 14–15).
(L) Cross-sections (plastic embedding) of the uppermost part of 6-day-old WT, *gLBD16-SRDX*, and *CASP1::shy2-2* roots. Four-day-old plants were treated for 48 h with mock or 1 μM NAA. As WT roots when treated with NAA keep forming LRs, it is rare (3/12) to have sections without LRs.
The yellow dots represent pericycle cells, the black dots represent periderm cells, and the double-headed black arrows indicate periderm extension. The yellow arrowheads indicate pericycle cell divisions. Black scale bars: 20 μm.
See also Figure S3 and Data S2.

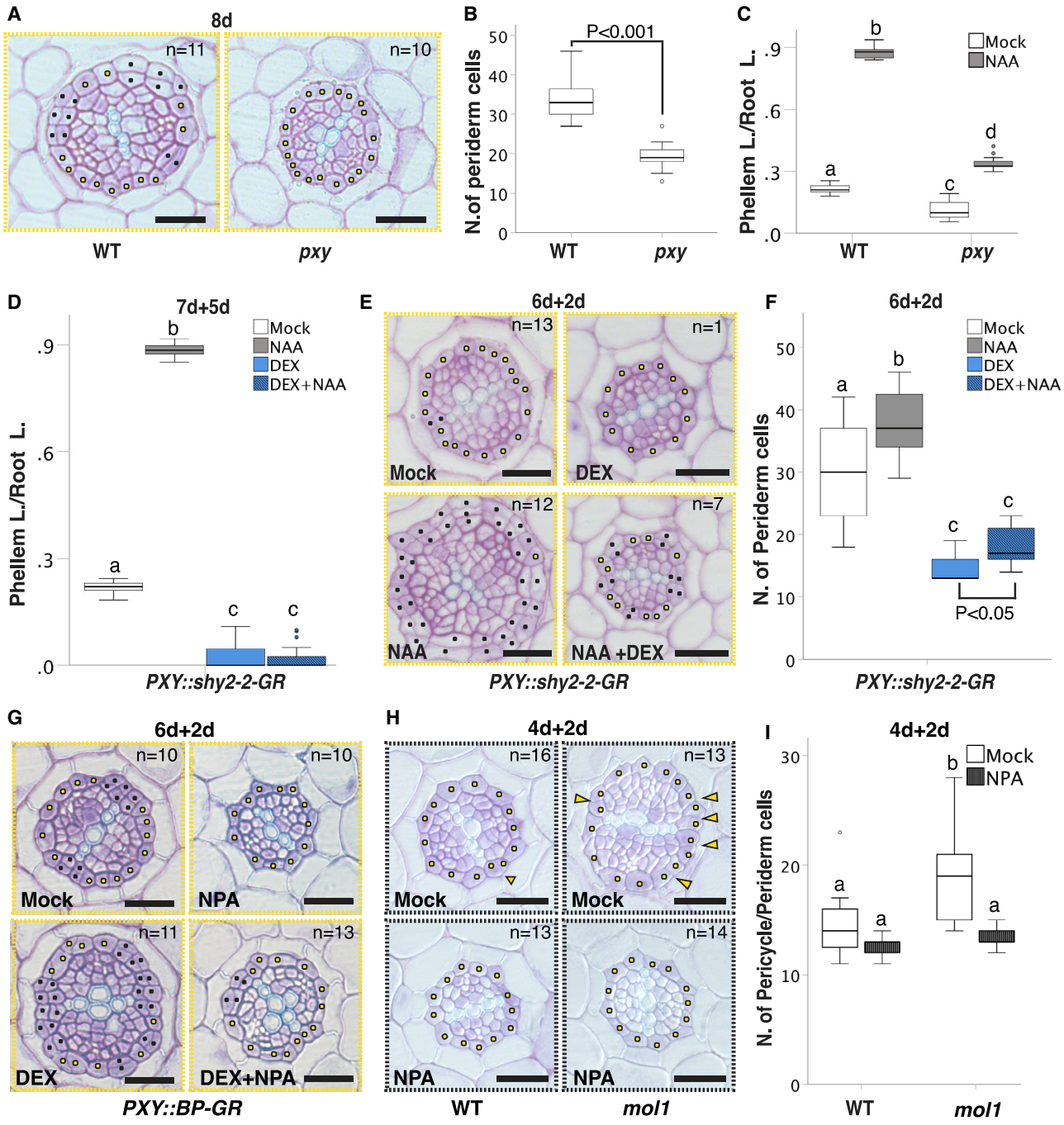

Figure 3. A Functional Vascular Cambium Is Required to Drive the Auxin-Induced Periderm Program

(A) Cross-sections (plastic embedding) of the uppermost part of 8-day-old WT and *pxy-3* roots.

(B) Quantification of number of pericycle/periderm cells in the experiment presented in (A); t test (n = 10–11).

(C) Quantification of phellem ratio in 12-day-old WT and *pxy-3* roots. Seven-day-old plants were treated for 5 days with mock or 1 μM NAA. One-way ANOVA (95% CI, post hoc: Tamhane, n = 14–15).

(D) Quantification of phellem ratio in 12-day-old roots of *PXY::shy2-2-GR* roots (in *MYB84::NLS-3xGFP W131Y*). Seven-day-old plants were treated for 5 days with mock, 1 μM NAA, 10 μM DEX, or 10 μM DEX + 1 μM NAA. One-way ANOVA (95% CI, post hoc: Tamhane, n = 15).

(E) Cross-sections (plastic embedding) of the uppermost part of *PXY::shy2-2-GR* (in *MYB84::NLS-3xGFP W131Y*) roots. Six-day-old plants were treated for 48 h with mock, 1 μM NAA, 10 μM DEX, or 10 μM DEX + 1 μM NAA.

(F) Quantification of number of pericycle/periderm cells in the experiment presented in (E). One-way ANOVA (95% CI, post hoc: Tamhane, n = 7–13) and t test.

(G) Cross-sections (plastic embedding) of the uppermost part of 6-day-old *PXY::BP-GR* roots. Four-day-old plants were treated for 48 h with mock, 10 μM DEX, 10 μM NPA, or 10 μM DEX + 10 μM NPA.

(H) Cross-sections (plastic embedding) of the uppermost part of 6-day-old WT and *mol1* roots. Four-day-old plants were treated for 48 h with mock or 10 μM NPA.

(legend continued on next page)

the auxin response in the periderm. Prolonged induction (5 days) of *PXY::shy2-2-GR* from 7 days onward resulted in delayed periderm formation and abolished auxin responses in the periderm (Figures 3D, S4D, and S4F). Consistently, 2-day induction at the onset of periderm/cambium initiation arrested both cambium and periderm formation, even in the presence of auxin, indicating that the establishment of the vascular cambium is required for periderm development (Figures 3E and 3F).

Next, we assumed that if the initiation of the vascular cambium renders the pericycle competent to form the periderm, high vascular cambium activity should promote periderm growth. To test this, we specifically overexpressed a master cambial regulator [29, 30] in the vascular cambium with temporal control (*PXY::BP-GR*). Induction of BREVIPEDICELLUS/KNAT1 (BP) from day 7 onward resulted in an increase in phellem length and phellem ratio (Figures S4G and S4H). Consistently, a short induction in the vascular cambium at the onset of periderm development was sufficient to promote both programs and this effect was attenuated by blocking auxin polar transport (Figures 3G and S4I). We reinforced these findings by investigating *more lateral growth1* (*mol1-1*) mutants, which are characterized by enhanced vascular cambium activity [31]. *MOL1* is solely expressed in the phloem and pro-cambium before the initiation of periderm development [31] (Figure S4J). At 6 days, *mol1-1* mutants already showed many pericycle cell divisions, and the total number of pericycle cells was increased compared to WT, indicating that periderm initiation occurred earlier (Figures 3H and 3I). NPA treatment suppressed the *mol1-1* phenotypes, highlighting the importance of auxin for both programs (Figures 3H, 3I, and S4K).

In summary, our results demonstrate that the vascular cambium is required and sufficient to promote periderm initiation. Thus, it may act as the developmental cue that renders the xylem pole pericycle competent to initiate the periderm program.

Distinct Targets Downstream of Auxin Orchestrate Periderm and LR Formation

We hypothesized that output distinction among the 2 developmental programs is also mediated by specificity in the auxin responses. To test this, we investigated whether the key auxin signaling components that regulate LR formation act during periderm development. Different auxin signaling modules comprising Aux/IAAs and auxin response factors (ARFs) regulated LR formation [12,26 32–38]. By mean of fluorescent reporters, we observed the activity of *IAA3/SHORT HYPOCOTYL 2 (SHY2)*, *IAA12/BODENLOS (BDL)*, *IAA28*, and *IAA14/SOLITARY ROOT (SLR)* promoters at all stages of periderm development (Figures 4A–4D). Genetic analysis exploiting gain-of-function mutants (stabilized versions) of the expressed IAAs [32–36] confirmed their role during periderm development. All of the mutants displayed decreased phellem length, decreased phellem ratio, and an impaired auxin response (Figures 4E–4G and S5A–S5C), with *bdl-2* and *shy2-101* being the most affected (Figures 4E). Also, at the anatomical level, *bdl-2* and *shy2-101* roots showed the strongest phenotype, with only 1–2 formed periderm layers and reduced overall secondary growth (Figures 4H–4J). In, *slr-1*, which totally lacks LRs [33] (Figure S5M) and displays only a mild reduction in the number of periderm layers (Figure 4I), the positive effect on blocking LR initiation on the periderm growth is suppressed/masked by altered auxin signaling in the periderm and/or by the absence of enhanced cambial activity.

Next, we examined whether *ARF5/MONOPTEROS (MP)*, *ARF6*, *ARF7/NPH4*, *ARF8*, and *ARF19*, which regulate LR development [26, 32, 34, 37, 38], also contribute to periderm growth. We showed that all of these *ARFs* are expressed in the periderm, albeit not at all periderm developmental stages (Figures 5A–5E, S5D, and S5E). We detected the activity of *ARF5* and *ARF8* promoters in a few phellogen cells only during late (stage 5) periderm development (Figures 5D, 5E, S5D, and S5E), whereas *ARF6*, *ARF7*, and *ARF19* promoter activity was observed during all stages of periderm development, including the first divisions in the pericycle (Figures 5A–5C). The comparison of the expression levels of these ARFs in the pericycle in the root at the positions corresponding to LR initiations and periderm initiation points out that ARF19 acts predominantly during LR formation, whereas ARF6 and ARF7 act in both processes. As ARF5 and ARF8 are very weakly expressed [8, 37, 39] and were at the border of detection at both positions, no assumptions could be made.

To further study whether output specificity is encoded by different ARFs, we investigated periderm development in *ARF* loss-of-function mutants. Our genetic studies revealed that *ARF8* and *MP/ARF5* are the major ARFs contributing to periderm formation, despite their low abundance (Figures 5F–5I, S5B, and S5F–S5I). Both an induced *amiMP* line (*mp/arf5* mutant fails to form a root, so we used an inducible artificial microRNA [miRNA] targeting *MP/ARF5* [8]) and the *arf8-2* single mutant showed a reduction in phellem length, phellem ratio, and auxin response (Figures 5F, 5G, S5F, and S5G). In addition, the number of periderm layers was reduced in the induced *amiMP* roots, whereas LR formation was not altered (Figures 5H, 5I, S5J, and S5K). In line with this, prolonged induction of MP at the onset of periderm formation resulted in increased phellem length, phellem ratio, and periderm layers (Figures 5J–5L and S5L). ARF5/MP, which contributes the most to periderm development, is known to activate vascular cambium formation in the root and repress cambium activity in the stem [8, 14], highlighting regulatory conservation between the 2 meristems. By contrast, the *arf7-1 arf19-1* double mutant, which totally lacks LRs (Figure S5M), showed normal cambium [8] and periderm growth, except for a reduced auxin response (Figures 4F, 5M, 5N, and S5B), highlighting that distinct auxin signaling modules do not equally contribute to periderm, LR, and cambium formation. Considering that the analyzed ARF loss-of-function mutants show only mild periderm defects, compared to IAA gain-of-function mutants, it is reasonable to think that either the analyzed ARFs work redundantly and/or additional ARFs are involved. To conclude, pericycle output specificity is only partially resolved

(I) Quantification of number of pericycle cells in the experiment presented in (H). One-way ANOVA (95% CI, post hoc: Tamhane, n = 13–16).
The yellow dots represent the pericycle cells, the black dots represent the periderm cells, and the yellow arrowheads indicate the pericycle divisions. Black scale bars: 20 μm.
See also Figure S4 and Data S2.

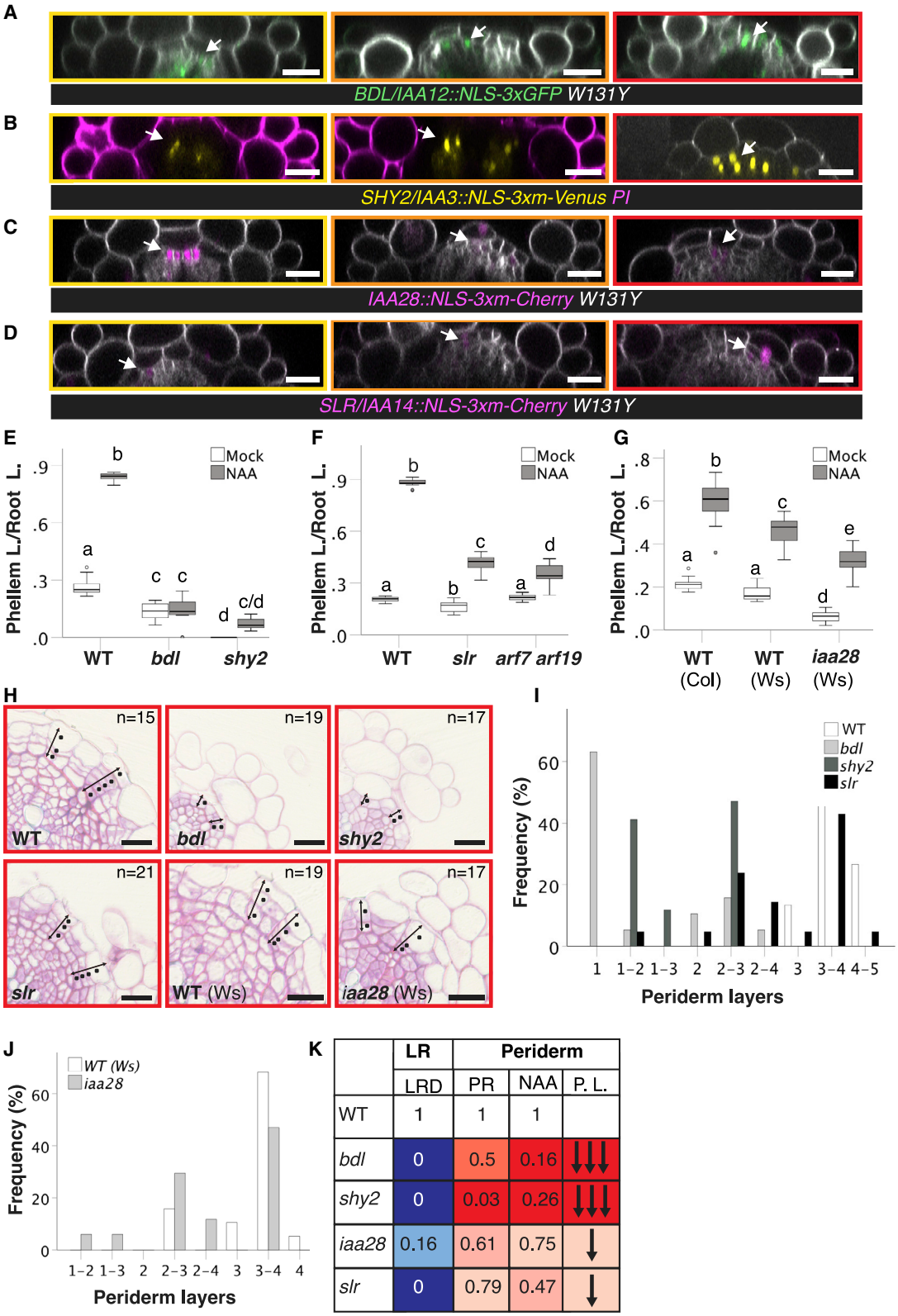

K

	LR	Periderm		
	LRD	PR	NAA	P. L.
WT	1	1	1	
bdl	0	0.5	0.16	↓↓↓
shy2	0	0.03	0.26	↓↓↓
iaa28	0.16	0.61	0.75	↓
slr	0	0.79	0.47	↓

(legend on next page)

by differences in the auxin signaling machinery involved in the 2 processes (Figures 4K and 5O).

Furthermore, we tested whether auxin-induced LR regulators function during periderm formation. The GATA23 TF specifies LR founder cell identity in xylem pole pericycle cells [32], whereas LBD16 together with other auxin-induced-LBD TFs regulate LR initiation, primordium growth, and emergence [24–26]. We determined their expression pattern during periderm development. The activity of *GATA23* and *LBD16* promoters was observed in the pericycle during LR initiation (Figures 6A and S6A) [26, 32], whereas it was at the border of detection in the pericycle at the onset of periderm initiation (Figures 6A and S6A). Consistently, the expression of *GATA23* and *LBD16* was not reduced in the periderm of *XPP::shy-2-2-GR*-induced roots as expected for an auxin target gene, and *gLBD16-SRDX* roots do not show any defects in the periderm, indicating that they do not play a major role during periderm development (Figure 6B). In the quest for factors downstream of auxin that regulate periderm growth, we selected known and putative MP/ARF5 targets [14, 40], restricting the list to *WOX4* and *BP/KNAT1* based on their expression during secondary growth [29, 41, 42]. We confirmed that both *WOX4* and *BP* are expressed all through periderm development (Figures S6B and S6C) and their expression is reduced in the periderm of *XPP::shy2-2-GR*-induced roots (Figure 6B). *WOX4* expression is excluded from the pericycle during LR initiation, whereas *BP* could still be detected, albeit at lower levels (Figures 6C and S6D).

To further explore their role during periderm development, we analyzed *BP* and *WOX4* loss-of-function mutants. Both the *wox4-1* and *bp-9* mutants displayed a reduction in phellem length and phellem ratio and impaired auxin response when compared to WT (Figures 6D and S6E). At the anatomical level, the number of periderm layers was reduced (Figures S6F and S6G), indicating that *WOX4* and *BP* control phellogen activity. In line with their specific role during secondary growth, *wox4-1* and *bp-9* mutants do not display any obvious LR phenotype (Figures S6H and S6I). To further confirm the specific contribution of *WOX4* and *BP* during periderm development, we generated *PER15::BP-GR* and *PER15::WOX4-GR* plants. Inducing *WOX4* and *BP* expression in the periderm of WT plants from 7 days onward (at the onset of periderm formation) resulted in roots with an increased phellem length, phellem ratio, and periderm layers compared to mock controls, confirming that *WOX4* and *BP* are periderm-positive regulators (Figures 6E–6H, S6J, and S6K).

DISCUSSION

Our genetic and gene expression data demonstrate that auxin promotes both LR and periderm initiation from the same tissue: the pericycle. LRs and the periderm arise by the reactivation of cell divisions in the pericycle at distinct root zones, and their initiation displays different temporal dynamics. While auxin signaling is required for the first formative cell divisions at the xylem pole pericycle of both developmental programs, auxin is not sufficient to elicit periderm inception, indicating that LR production is the main auxin-induced program (after plant greening/plant body establishment), and additional developmental cues are needed to trigger periderm development. In fact, the establishment of the vascular cambium is a prerequisite for auxin-activated periderm initiation, and precocious activation of the vascular cambium is sufficient to trigger periderm initiation. Moreover, the positive effect of blocking LR formation on periderm initiation may be related to cambium establishment, as in plants that lack LRs; precocious periderm initiation was accompanied by enhanced cambial activity. We suggest that a non-cell-autonomous signal (hormone/peptide/small RNA/mobile TF) triggered by the cambium renders the xylem pole pericycle competent to form a periderm by either directly specifying periderm identity or by amplifying the endogenous cues required for periderm specification. Alternatively, the establishment of the vascular cambium and the consequence radial expansion may generate mechanical forces on the pericycle, which could drive periderm initiation (Figure 7).

Recently, clonal analyses experiments showed that the vascular cambium arises from cells that are adjacent to the xylem, including xylem pole pericycle cells. Thus, the portion of the cambium in correspondence with the original xylem poles derives from the pericycle, whereas the remaining part originates from pro-cambial cells, which are near the xylem [8]. Xylem proximity is a prerequisite only for vascular cambium formation and not for phellogen establishment, while auxin signaling is required in both processes, adding another level of complexity to the

Figure 4. Distinct IAAs Contribute to Periderm Development

(A–D) Orthogonal view of z stacks of *BDL/IAA12::NLS-3xGFP W131Y* (A), *SHY2/IAA3::NLS-3xm-Venus* (B), *IAA28::NLS-3xm-Cherry W131Y* (C), and *SLR/IAA14::NLS-3xm-Cherry W131Y* (D). Twelve-day-old roots at the positions corresponding to stage 1 (left panel), stages 3/4 (center panel), and stage 5 (right panel) of periderm development.

(E) Quantification of phellem ratio in 12-day-old WT, *bdl-2*, and *shy2-201* roots. Seven-day-old plants were treated for 5 days with mock or 1 μM NAA. One-way ANOVA (95% CI, post hoc: Tamhane, n = 8–14).

(F) Quantification of phellem ratio in 12-day-old WT, *slr-1*, and *arf7-1 arf19-1* roots. Seven-day-old plants were treated for 5 days with mock or 1 μM NAA. One-way ANOVA (95% CI, post hoc: Tamhane, n = 14–15).

(G) Quantification of phellem ratio in 10-day-old WT (Ws and Col) and *iaa28-1*(Ws) roots. Seven-day-old plants were treated for 3 days with mock or 1 μM NAA. One-way ANOVA (95% CI, post hoc: Tamhane, n = 14).

(H) Cross-sections (plastic embedding) of the uppermost part of 12-day-old WT, *bdl-2*, *shy2-201*, *slr-1*, WT (WS), and *iaa28-1* roots.

(I and J) Quantification of the number of periderm layers of (H).

(K) Table comparing *IAA* root phenotypes. Mutant phenotypes were normalized to WT, which was set to 1. LRD, lateral root density; PR, phellem ratio; NAA, auxin response (PR mock/PR NAA); and P.L., number of periderm layers.

The white arrows indicate the pericycle/phellogen, the double-headed black arrows indicate the periderm extension, and the black dots indicate the periderm layers. Black and white scale bars: 20 μm.

See also Figure S5 and Data S2.

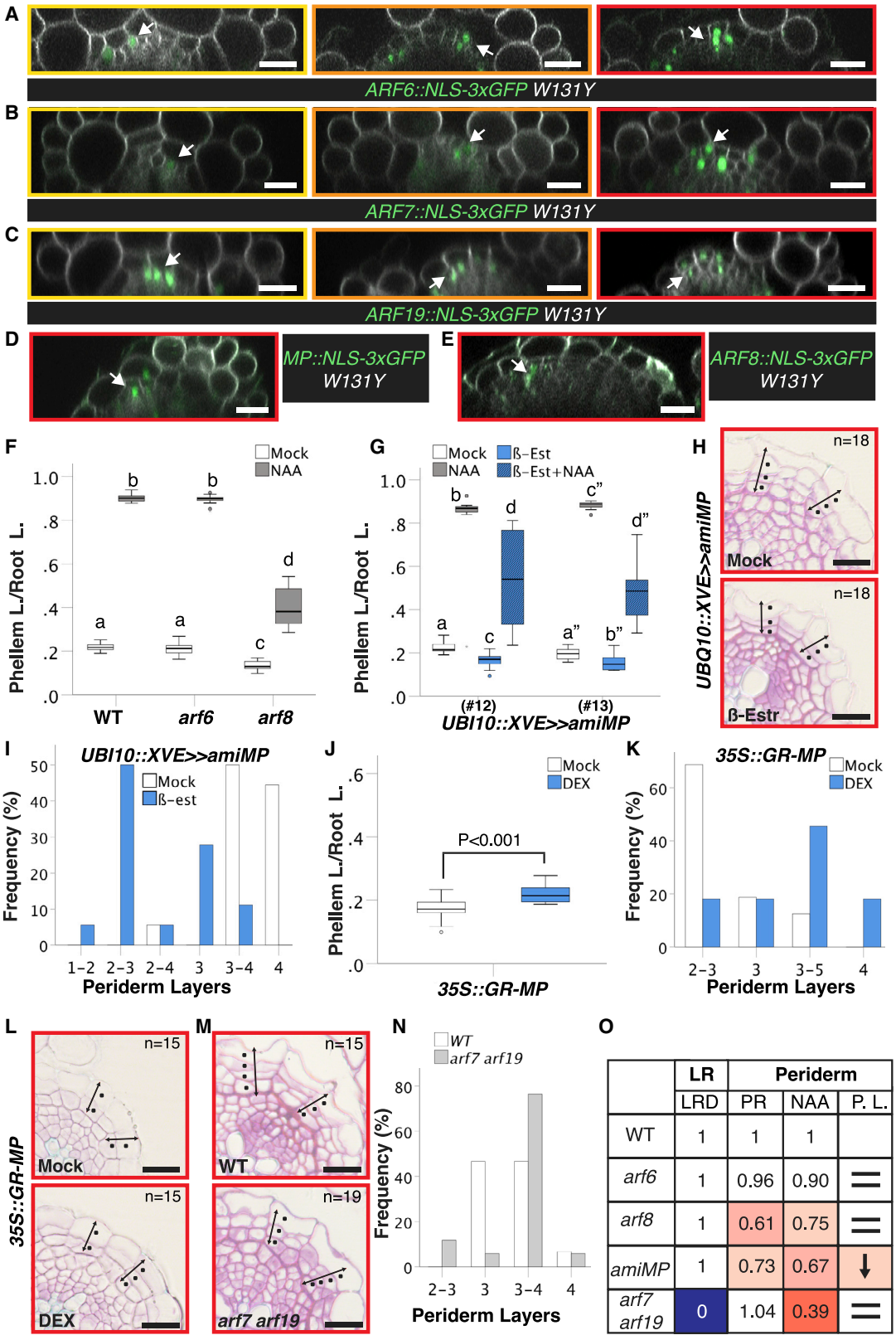

	LR	Periderm		
	LRD	PR	NAA	P. L.
WT	1	1	1	
arf6	1	0.96	0.90	=
arf8	1	0.61	0.75	=
amiMP	1	0.73	0.67	↓
arf7 arf19	0	1.04	0.39	=

Figure 5. Distinct ARFs Contribute to Periderm Development

(A–C) Orthogonal view of z stacks of *ARF6::NLS-3xGFP W131Y* (A), *ARF7::NLS-3xGFP W131Y* (B), and *ARF19::NLS-3xGFP W131Y* (C) 12-day-old roots at the positions corresponding to stage 1 (left panels), stages 3/4 (center panels), and stage 5 (right panels) of periderm development.

(legend continued on next page)

system [8]. Studies with single-cell resolution and temporal dynamics are necessary to further dissect how the 3 programs are connected, and, especially, whether LRs influence the establishment of the vascular cambium and how the phellogen and the vascular cambium are specified from xylem pole pericycle cells. In addition, LR initiation is strongly controlled by nutrient availability; therefore, it will be interesting to explore whether environmental stimuli influence pericycle developmental transitions.

We highlighted that distinct signaling pathways, downstream of auxin, orchestrate periderm and LR formation. We showed that MP, which also regulates cambium activity via WOX4 [8, 14], and ARF8 are the majors ARFs contributing to periderm formation, whereas the key LR module SLR-ARF7-ARF19 [26, 38] plays only a minor role during periderm growth. However, it is likely that other ARFs or other ARF combinations participate in periderm development, as the loss of function of ARF8 or conditionally knocking down MP only lead to mild periderm phenotypes. We found that downstream of ARFs during periderm development, WOX4 and BP play a prominent role in controlling meristem activity, highlighting distinction from the LR program and major overlaps between the vascular cambium and the phellogen networks (Figure 7). Periderm-specific overexpression of *WOX4* and *BP* provides a novel approach for increasing periderm layers, a trait that is known to contribute to stress tolerance [3, 43]. Another key aspect for breeding programs is that WOX4 and BP are sufficient to increase cambial activity [30], paving the way for programs targeting simultaneously biomass and resistance to abiotic stresses. In this regard, it would be interesting to further decipher the complex molecular mechanisms coordinating the activity of the phellogen and the vascular cambium.

STAR★METHODS

Detailed methods are provided in the online version of this paper and include the following:

SUPPLEMENTAL INFORMATION

Supplemental Information can be found online at https://doi.org/10.1016/j.cub.2020.08.053.

ACKNOWLEDGMENTS

We thank Stefan Mann for cloning the *PER15* promoter in GreenGate. We thank Marja Timmermans, Antia Rodriguez-Villalon, and Ari Pekka Mähönen for critical reading of the manuscript. We thank Andrea Boch for technical help. Work in the Vermeer lab is supported by grants from the Swiss National Science Foundation (Schweizerischer Nationalfonds zur Förderung der Wissenschaftlichen Forschung, PP00P3_157524 and 316030_164086) and the Netherlands Organisation for Scientific Research (Nederlandse Organisatie voor Wetenschappelijk Onderzoek, NWO 864.13.008). Work in the Ragni lab was supported by the Deutsche Forschungsgemeinschaft (DFG grant RA-2590/1-2).

AUTHOR CONTRIBUTIONS

W.X. planned and conducted the majority of the experiments with input from L.R. L.R. and W.X. acquired the confocal images. A.W. conducted the initial experiments on the *arf* and *iaa* mutants. D.M., L.R., and W.X. did the molecular cloning and generated the plant lines. D.M. conducted the Fluorol Yellow (FY) experiments. W.X. and D.M. measured the number of periderm layers. A.W., W.X., and D.M. conducted the phellem ratio experiments. D.R. helped in generating the T3 lines and in the embedding of some experiments. J.E.M.V. provided the PER15 promoter and significant input to the project. L.R. wrote the manuscript, with the help of W.X., D.M., A.W., and J.E.M.V.

(D and E), Orthogonal view of z stacks of *ARF5/MP::NLS-3xGFP W131Y* (D) and *ARF8::NLS-3xGFP W131Y* (E). Twelve-day-old roots at the position corresponding to stage 5 of periderm development.
(F) Quantification of phellem ratio in 12-day-old WT, *arf6-1*, and *arf8-2* roots. Seven-day-old plants were treated for 5 days with mock or 1 μM NAA. One-way ANOVA (95% CI, post hoc: Tamhane, n = 15–16).
(G) Quantification of phellem ratio in *UBI10::XVE>>amiMP* lines. Seven-day-old plants were treated for 5 days with mock, 1 μM NAA, 5 μM β-estradiol (β-Estr) or 5 μM β-Estr + 1 μM NAA. One-way ANOVA (95% CI, post hoc: Tamhane, n = 12–14).
(H) Cross-sections (plastic embedding) of the uppermost part of 12-day-old *amiMP* (#13) roots. Seven-day-old plants were treated for 5 days with mock or 5 μM β-Estr.
(I) Quantification of the number of periderm layers of the experiment shown in (H).
(J) Quantification of phellem ratio in *35S::GR-MP* roots. Seven-day-old plants were treated for 5 days with mock or 10 μM DEX; t test (n = 15).
(K) Quantification of the number of periderm layers of the experiment shown in (L).
(L) Cross-sections (plastic embedding) of the uppermost part of 12-day-old *35S::GR-MP* roots. Seven-day-old plants were treated for 5 days with mock or 10 μM DEX.
(M) Cross-sections roots (plastic embedding) of the uppermost part of WT and *arf7-1-arf19-1* 12-day-old roots.
(N) Quantification of the number of periderm layers of the experiment shown in (M).
(O) Table comparing *ARF* phenotypes in the root. Mutant phenotypes were normalized to WT, which was set to 1. LRD, lateral root density; PR, phellem ratio; NAA, auxin response (PR mock/PR NAA); and P.L., number of periderm layers.
The white arrows indicate the pericycle/phellogen, the double-headed black arrows indicate the periderm extension, and the black dots indicate the periderm layers. Black and white scale bars: 20 μm.
See also Figure S5 and Data S2.

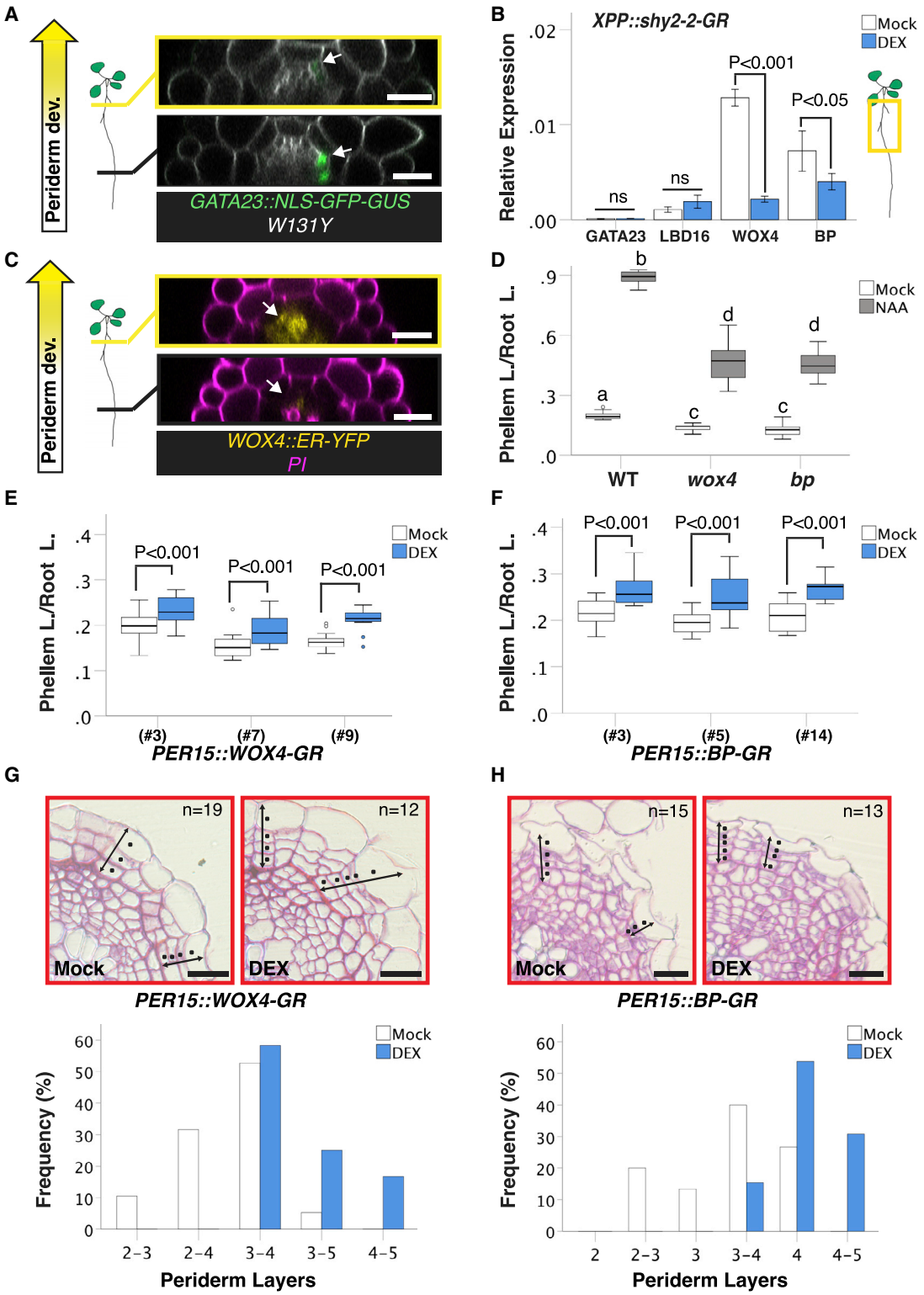

Figure 6. Distinct Targets Downstream of Auxin Orchestrate Periderm and LR Formation

(A) Orthogonal view of z stacks of a *GATA23::NLS-GFP-GUS W131Y* 7-day-old root at the positions corresponding to LR primordia (bottom) and stage 1 of periderm development (top).

(B) Relative expression of *LBD16*, *GATA23*, *WOX4*, and *BP/KNAT1* in the periderm of *XPP::shy2-2-GR* (in *MYB84::NLS-3xGFP W131Y*; #1) roots. Seven-day-old plants were treated for 2 days with mock or 10 μM DEX. The bars represent the means and the error bars represent ±2 SE; t test (ns, not significant; n = 3–4).

(C) Orthogonal view of z stacks of a *WOX4::ER-YFP* 7-day-old root at the positions corresponding to LR primordia (bottom) and stage 1 (top).

(legend continued on next page)

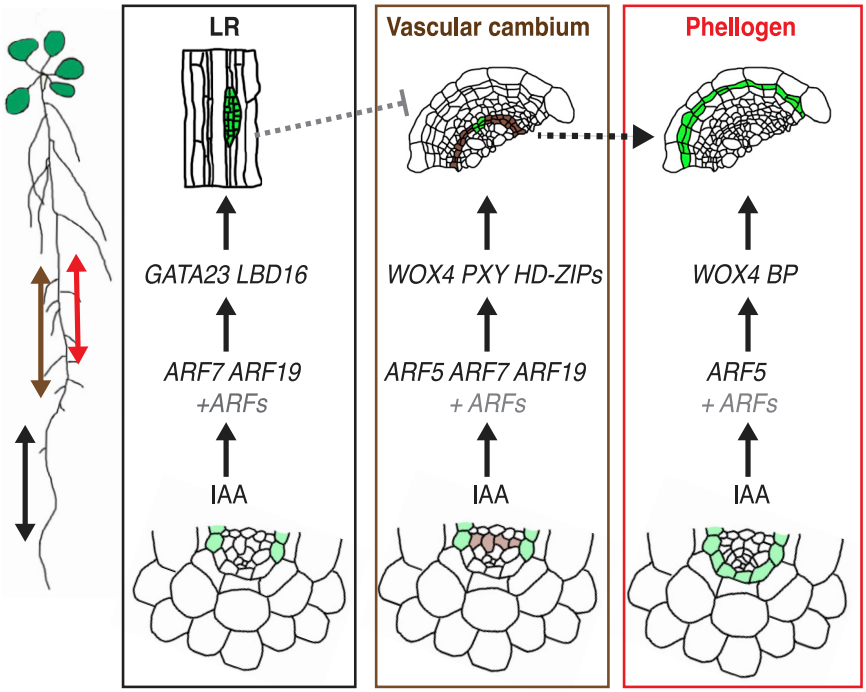

Figure 7. Model Explaining Pericycle Output Specificity

LRs, the phellogen, and part of the vascular cambium arise from reactivation of divisions in the pericycle. Auxin promotes these 3 programs. LR formation is the main auxin-induced program in the pericycle after the plant body is established. ARF7 and ARF19 are the main ARFs that activate GATA23 and LBDs, and thus the LR program. Auxin promotes phellogen formation via ARF5 and ARF8 (and probably other ARFs) and through the activation of WOX4 and BP. The establishment of the vascular cambium, which is also regulated by auxin via MP, WOX4, PXY, and HD-ZIPs, is required for periderm formation (the vascular cambium scheme is based on data in [8]).

The double-headed black arrow indicates the zone of the root where LR are specified and initiated, the double-headed red arrow indicates the zone of the root where periderm establishment occurs, and the double-headed brown arrow is where the vascular cambium is established. Gene names and arrows in gray indicate proposed interactions. The pericycle cells are depicted in pale green, the cells derived from the pericycle are depicted in green, the pro-cambial cells are in pale brown, and the cells derived from the pro-cambium are depicted in brown.

DECLARATION OF INTERESTS

The authors declare no competing interests.

Received: May 2, 2020
Revised: July 22, 2020
Accepted: August 14, 2020
Published: September 10, 2020

REFERENCES

1. Ragni, L., and Greb, T. (2018). Secondary growth as a determinant of plant shape and form. Semin. Cell Dev. Biol. *79*, 58–67.
2. Shi, D., Lebovka, I., López-Salmerón, V., Sanchez, P., and Greb, T. (2019). Bifacial cambium stem cells generate xylem and phloem during radial plant growth. Development *146*, dev171355.
3. Campilho, A., Nieminen, K., and Ragni, L. (2020). The development of the periderm: the final frontier between a plant and its environment. Curr. Opin. Plant Biol. *53*, 10–14.
4. Esau, K. (1965). Plant Anatomy (John Wiley & Sons).
5. Machado, A., Pereira, H., and Teixeira, R.T. (2013). Anatomy and development of the endodermis and phellem of Quercus suber L. roots. Microsc. Microanal. *19*, 525–534.
6. Wunderling, A., Ripper, D., Barra-Jimenez, A., Mahn, S., Sajak, K., Targem, M.B., and Ragni, L. (2018). A molecular framework to study periderm formation in Arabidopsis. New Phytol. *219*, 216–229.
7. Dolan, L., Janmaat, K., Willemsen, V., Linstead, P., Poethig, S., Roberts, K., and Scheres, B. (1993). Cellular organisation of the Arabidopsis thaliana root. Development *119*, 71–84.
8. Smetana, O., Mäkilä, R., Lyu, M., Amiryousefi, A., Sánchez Rodríguez, F., Wu, M.F., Solé-Gil, A., Leal Gavarrón, M., Siligato, R., Miyashima, S., et al. (2019). High levels of auxin signalling define the stem-cell organizer of the vascular cambium. Nature *565*, 485–489.
9. Du, Y., and Scheres, B. (2018). Lateral root formation and the multiple roles of auxin. J. Exp. Bot. *69*, 155–167.
10. Vermeer, J.E., von Wangenheim, D., Barberon, M., Lee, Y., Stelzer, E.H., Maizel, A., and Geldner, N. (2014). A spatial accommodation by neighboring cells is required for organ initiation in Arabidopsis. Science *343*, 178–183.
11. Escamez, S., André, D., Sztojka, B., Bollhöner, B., Hall, H., Berthet, B., Voß, U., Lers, A., Maizel, A., Andersson, M., et al. (2020). Cell Death in Cells Overlying Lateral Root Primordia Facilitates Organ Growth in Arabidopsis. Curr. Biol. *30*, 455–464.e7.
12. Leyser, O. (2018). Auxin Signaling. Plant Physiol. *176*, 465–479.

(D) Quantification of phellem ratio of 12-day-old WT, *wox4-1*, and *bp-9* roots. Seven-day-old plants were treated for 5 days with mock or 1 μM NAA. One-way ANOVA (95% CI, post hoc: Tamhane, n = 15–16).
(E) Quantification of phellem ratio in 3 independent *PER15::WOX4-GR* (in *W131Y*) T2 lines. Seven-day-old plants were treated for 5 days with mock or 10 μM DEX; t test (n = 14–16).
(F) Quantification of phellem ratio in 3 independent *PER15::BP-GR* lines. Seven-day-old plants were treated for 5 days with mock or 10 μM DEX; t test (n = 14–15).
(G) Top: cross-sections (plastic embedding) of the uppermost part of *PER15::WOX4-GR* (in *W131Y*; #3) roots: mock (left panel), 10 μM DEX induced (right panel). Seven-day-old plants were treated for 5 days with mock or 10 μM DEX. Bottom: quantification of the number of periderm layers in *PER15::WOX4-GR* (in *W131Y; #3*) of the experiment.
(H) Top: cross-sections of the uppermost part of *PER15::BP-GR* (#3) roots (plastic embedding): mock (left panel), 10 μM DEX induced (right panel). Seven-day-old plants were treated for 5 days with mock or 10 μM DEX. Bottom: quantification of the number of periderm layers in *PER15::BP-GR* (*#3*) of the experiment.
The white arrows indicate the pericycle, the double-headed black arrows indicate the periderm extension, and the black dots indicate the periderm cells. Black and white scale bars: 20 μm.
See also Figure S6 and Data S2.

13. Yamaguchi, Y.L., Ishida, T., and Sawa, S. (2016). CLE peptides and their signaling pathways in plant development. J. Exp. Bot. *67*, 4813–4826.
14. Brackmann, K., Qi, J., Gebert, M., Jouannet, V., Schlamp, T., Grünwald, K., Wallner, E.-S., Novikova, D.D., Levitsky, V.G., Agustí, J., et al. (2018). Spatial specificity of auxin responses coordinates wood formation. Nat. Commun. *9*, 875.
15. Di Mambro, R., De Ruvo, M., Pacifici, E., Salvi, E., Sozzani, R., Benfey, P.N., Busch, W., Novak, O., Ljung, K., Di Paola, L., et al. (2017). Auxin minimum triggers the developmental switch from cell division to cell differentiation in the *Arabidopsis* root. Proc. Natl. Acad. Sci. USA *114*, E7641–E7649.
16. Motte, H., Vanneste, S., and Beeckman, T. (2019). Molecular and Environmental Regulation of Root Development. Annu. Rev. Plant Biol. *70*, 465–488.
17. Smit, M.E., and Weijers, D. (2015). The role of auxin signaling in early embryo pattern formation. Curr. Opin. Plant Biol. *28*, 99–105.
18. Liao, C.Y., Smet, W., Brunoud, G., Yoshida, S., Vernoux, T., and Weijers, D. (2015). Reporters for sensitive and quantitative measurement of auxin response. Nat. Methods *12*, 207–210.
19. Ramakrishna, P., Ruiz Duarte, P., Rance, G.A., Schubert, M., Vordermaier, V., Vu, L.D., Murphy, E., Vilches Barro, A., Swarup, K., Moirangthem, K., et al. (2019). EXPANSIN A1-mediated radial swelling of pericycle cells positions anticlinal cell divisions during lateral root initiation. Proc. Natl. Acad. Sci. USA *116*, 8597–8602.
20. Andersen, T.G., Naseer, S., Ursache, R., Wybouw, B., Smet, W., De Rybel, B., Vermeer, J.E.M., and Geldner, N. (2018). Diffusible repression of cytokinin signalling produces endodermal symmetry and passage cells. Nature *555*, 529–533.
21. Ueda, K., Matsuyama, T., and Hashimoto, T. (1999). Visualization of microtubules in living cells of transgenic Arabidopsis thaliana. Protoplasma *206*, 201–206.
22. Boerjan, W., Cervera, M.T., Delarue, M., Beeckman, T., Dewitte, W., Bellini, C., Caboche, M., Van Onckelen, H., Van Montagu, M., and Inzé, D. (1995). Superroot, a recessive mutation in Arabidopsis, confers auxin overproduction. Plant Cell *7*, 1405–1419.
23. Mikkelsen, M.D., Naur, P., and Halkier, B.A. (2004). Arabidopsis mutants in the C-S lyase of glucosinolate biosynthesis establish a critical role for indole-3-acetaldoxime in auxin homeostasis. Plant J. *37*, 770–777.
24. Goh, T., Joi, S., Mimura, T., and Fukaki, H. (2012). The establishment of asymmetry in Arabidopsis lateral root founder cells is regulated by LBD16/ASL18 and related LBD/ASL proteins. Development *139*, 883–893.
25. Lee, H.W., Kim, N.Y., Lee, D.J., and Kim, J. (2009). LBD18/ASL20 regulates lateral root formation in combination with LBD16/ASL18 downstream of ARF7 and ARF19 in Arabidopsis. Plant Physiol. *151*, 1377–1389.
26. Okushima, Y., Fukaki, H., Onoda, M., Theologis, A., and Tasaka, M. (2007). ARF7 and ARF19 regulate lateral root formation via direct activation of LBD/ASL genes in Arabidopsis. Plant Cell *19*, 118–130.
27. Fisher, K., and Turner, S. (2007). PXY, a receptor-like kinase essential for maintaining polarity during plant vascular-tissue development. Curr. Biol. *17*, 1061–1066.
28. Hirakawa, Y., Shinohara, H., Kondo, Y., Inoue, A., Nakanomyo, I., Ogawa, M., Sawa, S., Ohashi-Ito, K., Matsubayashi, Y., and Fukuda, H. (2008). Non-cell-autonomous control of vascular stem cell fate by a CLE peptide/receptor system. Proc. Natl. Acad. Sci. USA *105*, 15208–15213.
29. Liebsch, D., Sunaryo, W., Holmlund, M., Norberg, M., Zhang, J., Hall, H.C., Helizon, H., Jin, X., Helariutta, Y., Nilsson, O., et al. (2014). Class I KNOX transcription factors promote differentiation of cambial derivatives into xylem fibers in the Arabidopsis hypocotyl. Development *141*, 4311–4319.
30. Zhang, J., Eswaran, G., Alonso-Serra, J., Kucukoglu, M., Xiang, J., Yang, W., Elo, A., Nieminen, K., Damén, T., Joung, J.G., et al. (2019). Transcriptional regulatory framework for vascular cambium development in Arabidopsis roots. Nat. Plants *5*, 1033–1042.
31. Agusti, J., Lichtenberger, R., Schwarz, M., Nehlin, L., and Greb, T. (2011). Characterization of transcriptome remodeling during cambium formation identifies MOL1 and RUL1 as opposing regulators of secondary growth. PLOS Genet. *7*, e1001312.
32. De Rybel, B., Vassileva, V., Parizot, B., Demeulenaere, M., Grunewald, W., Audenaert, D., Van Campenhout, J., Overvoorde, P., Jansen, L., Vanneste, S., et al. (2010). A novel aux/IAA28 signaling cascade activates GATA23-dependent specification of lateral root founder cell identity. Curr. Biol. *20*, 1697–1706.
33. Fukaki, H., Tameda, S., Masuda, H., and Tasaka, M. (2002). Lateral root formation is blocked by a gain-of-function mutation in the SOLITARY-ROOT/IAA14 gene of Arabidopsis. Plant J. *29*, 153–168.
34. Goh, T., Kasahara, H., Mimura, T., Kamiya, Y., and Fukaki, H. (2012). Multiple AUX/IAA-ARF modules regulate lateral root formation: the role of Arabidopsis SHY2/IAA3-mediated auxin signalling. Philos. Trans. R. Soc. Lond. B Biol. Sci. *367*, 1461–1468.
35. Hayward, A., Stirnberg, P., Beveridge, C., and Leyser, O. (2009). Interactions between auxin and strigolactone in shoot branching control. Plant Physiol. *151*, 400–412.
36. Rogg, L.E., Lasswell, J., and Bartel, B. (2001). A gain-of-function mutation in IAA28 suppresses lateral root development. Plant Cell *13*, 465–480.
37. De Smet, I., Lau, S., Voss, U., Vanneste, S., Benjamins, R., Rademacher, E.H., Schlereth, A., De Rybel, B., Vassileva, V., Grunewald, W., et al. (2010). Bimodular auxin response controls organogenesis in Arabidopsis. Proc. Natl. Acad. Sci. USA *107*, 2705–2710.
38. Okushima, Y., Overvoorde, P.J., Arima, K., Alonso, J.M., Chan, A., Chang, C., Ecker, J.R., Hughes, B., Lui, A., Nguyen, D., et al. (2005). Functional genomic analysis of the AUXIN RESPONSE FACTOR gene family members in Arabidopsis thaliana: unique and overlapping functions of ARF7 and ARF19. Plant Cell *17*, 444–463.
39. Hardtke, C.S., Ckurshumova, W., Vidaurre, D.P., Singh, S.A., Stamatiou, G., Tiwari, S.B., Hagen, G., Guilfoyle, T.J., and Berleth, T. (2004). Overlapping and non-redundant functions of the Arabidopsis auxin response factors MONOPTEROS and NONPHOTOTROPIC HYPOCOTYL 4. Development *131*, 1089–1100.
40. O'Malley, R.C., Huang, S.C., Song, L., Lewsey, M.G., Bartlett, A., Nery, J.R., Galli, M., Gallavotti, A., and Ecker, J.R. (2016). Cistrome and Epicistrome Features Shape the Regulatory DNA Landscape. Cell *165*, 1280–1292.
41. Hirakawa, Y., Kondo, Y., and Fukuda, H. (2010). TDIF peptide signaling regulates vascular stem cell proliferation via the WOX4 homeobox gene in Arabidopsis. Plant Cell *22*, 2618–2629.
42. Suer, S., Agusti, J., Sanchez, P., Schwarz, M., and Greb, T. (2011). WOX4 imparts auxin responsiveness to cambium cells in Arabidopsis. Plant Cell *23*, 3247–3259.
43. Thangavel, T., Tegg, R.S., and Wilson, C.R. (2016). Toughing It Out–Disease-Resistant Potato Mutants Have Enhanced Tuber Skin Defenses. Phytopathology *106*, 474–483.
44. Geldner, Niko, Dénervaud-Tendon, Valerie, Hyman, D.L., Mayer, U., Stierhof, Y.-D., and Chory, J. (2009). Rapid, combinatorial analysis of membrane compartments in intact plants with a multicolor marker set. Plant J *59*, 169–178.
45. Rademacher, E.H., Moller, B., Lokerse, A.S., Llavata-Peris, C.I., van den Berg, W., and Weijers, D. (2011). A cellular expression map of the Arabidopsis AUXIN RESPONSE FACTOR gene family. Plant J *68*, 597–606.
46. Ito, J., Fukaki, H., Onoda, M., Li, L., Li, C., Tasaka, M., et al. (2016). Auxin-dependent compositional change in Mediator in ARF7- and ARF19-mediated transcription. Proc. Nat. Acad. Sci. U.S.A. *113*, 6562–6567.

47. Smith, H.M., and Hake, S. (2003). The interaction of two homeobox genes, BREVIPEDICELLUS and PENNYWISE, regulates internode patterning in the Arabidopsis inflorescence. Plant Cell *15*, 1717–1727.

48. Agusti, J., Herold, S., Schwarz, M., Sanchez, P., Ljung, K., Dun, E.A., et al. (2011). Strigolactone signaling is required for auxin-dependent stimulation of secondary growth in plants. Proc. Natl. Acad. Sci. U.S.A. *108*, 20242–20247.

49. Gursanscky, N.R., Jouannet, V., Grunwald, K., Sanchez, P., Laaber-Schwarz, M., and Greb, T. (2016). MOL1 is required for cambium homeostasis in Arabidopsis. Plant J *86*, 210–220.

50. Vilches Barro, A., Stockle, D., Thellmann, M., Ruiz-Duarte, P., Bald, L., Louveaux, M., et al. (2019). Cytoskeleton Dynamics Are Necessary for Early Events of Lateral Root Initiation in Arabidopsis. Curr. Biol. *29*, 2443–2454.

51. Ulmasov, T., Murfett, J., Hagen, G., and Guilfoyle, T.J. (1997). Aux/IAA proteins repress expression of reporter genes containing natural and highly active synthetic auxin response elements. Plant Cell *9*, 1963–1971.

52. Schindelin, J., Arganda-Carreras, I., Frise, E., Kaynig, V., Longair, M., Pietzsch, T., Preibisch, S., Rueden, C., Saalfeld, S., Schmid, B., et al. (2012). Fiji: an open-source platform for biological-image analysis. Nat. Methods *9*, 676–682.

53. Lampropoulos, A., Sutikovic, Z., Wenzl, C., Maegele, I., Lohmann, J.U., and Forner, J. (2013). GreenGate—a novel, versatile, and efficient cloning system for plant transgenesis. PLOS ONE *8*, e83043.

54. Schürholz, A.K., López-Salmerón, V., Li, Z., Forner, J., Wenzl, C., Gaillochet, C., Augustin, S., Barro, A.V., Fuchs, M., Gebert, M., et al. (2018). A Comprehensive Toolkit for Inducible, Cell Type-Specific Gene Expression in Arabidopsis. Plant Physiol. *178*, 40–53.

55. de Reuille, P.B., and Ragni, L. (2017). Vascular Morphodynamics During Secondary Growth. Methods Mol. Biol. *1544*, 103–125.

56. Naseer, S., Lee, Y., Lapierre, C., Franke, R., Nawrath, C., and Geldner, N. (2012). Casparian strip diffusion barrier in Arabidopsis is made of a lignin polymer without suberin. Proc. Natl. Acad. Sci. USA *109*, 10101–10106.

STAR★METHODS

KEY RESOURCES TABLE

REAGENT or RESOURCE	SOURCE	IDENTIFIER
Bacterial and Virus Strains		
Escherichia coli DH5alfa	Widely distributed	N/A
Agrobacterium tumefaciens GV3101	Widely distributed	N/A
Chemicals, Peptides, and Recombinant Proteins		
Indole-3-acetic acid (IAA)	Duchefa	Cat# I0901
1-Naphthaleneacetic acid (NAA)	Duchefa	Cat# N0903
N-1-naphthylphthalamic acid (NPA)	Duchefa	Cat# N0926
Dexamethasone (DEX)	Sigma	Cat# D1756
β-Estradiol (β-Estr.)	Sigma	Cat# E8875
Propidium Iodide (PI)	Sigma	Cat# P4864
Murashige and Skoog Basal Medium (MS)	Duchefa	Cat# M0255
Plant Agar	Duchefa	Cat# P1001.1000
2,4-Dichlorophenoxyacetic acid (2,4 D)	Sigma	Cat# D-7299
Technovit 7100	Heraeus Kulzer	Cat# 64709003
Fluorol yellow (FY)	Santa Cruz	Cat# sc-215052
X-Glux	Duchefa	Cat# X-1405
Toluidine blue	Sigma	Cat# T3260
Chloral hydrate	Merck	Cat# 1.02425.1000
Glycerol	Roth	Cat# 6962.1
Critical Commercial Assays		
The Universal RNA Purification Kit	Roboklon	Cat# E3598-02
AMV Reverse Transcriptase Native	Roboklon	Cat# E1372-01
MESA blue	Eurogentec	Cat# RT-SYS2X-03+NRWOUB
Experimental Models: Organisms/Strains		
Arabidopsis: Col-0	Widely distributed	N/A
Arabidopsis: Ws	Widely distributed	N/A
Arabidopsis: *MYB84::NLS-3xGFP* in W131Y	[6]	N/A
Arabidopsis: *UBQ10::eYFP-NPSN12 (W131Y)*	[44]	N/A
Arabidopsis: *R2D2 (RPS5A::m-D2-dTomato>>RPS5A::D2VENUS)* in Col-0	[18]	N/A
Arabidopsis: *ARF7::NLS-3xGFP* in Col-0	[45]	NASC: N67080
Arabidopsis: *ARF19::NLS-3xGFP* in Col-0	[45]	NASC: N67104
Arabidopsis: *ARF8::NLS-3xGFP* in Col-0	[45]	NASC: N67082

(*Continued on next page*)

Continued

REAGENT or RESOURCE	SOURCE	IDENTIFIER
Arabidopsis: *ARF6::NLS-3xGFP* in Col-0	[45]	NASC: N67078
Arabidopsis: *ARF5::NLS-3xGFP* in Col-0	[45]	NASC: N67076
Arabidopsis: *IAA28::NLS-3xm-Cherry* in *MYB84::NLS-3xGFP* W131Y	This manuscript	N/A
Arabidopsis: *SLR/IAA14::NLS-3xm-Cherry* in *MYB84::NLS-3xGFP* in W131Y	This manuscript	N/A
Arabidopsis: *BDL/IAA12::NLS-3xGFP*	[37]	N/A
Arabidopsis: *SHY2/IAA2::NLS-3xm-Venus*	[10]	N/A
Arabidopsis: *LBD16::GUS* in Col-0	[46]	N/A
Arabidopsis: *DR5v2::ER-YFP* in Col-0	[14]	N/A
Arabidopsis: *shy2-101* in Col-0	[34]	N/A
Arabidopsis: *bdl-2* in Col-0	[35]	N/A
Arabidopsis: *GATA23::NLS-GFP-GUS*	[32]	N/A
Arabidopsis: *iaa28-1* in Ws	[36]	N/A
Arabidopsis: *arf7-1 arf19-1*	[38]	NASC: N24629
Arabidopsis: *slr-1* in Col-0	[33]	N/A
Arabidopsis: *arf8-3* in Col-0	[38]	N/A
Arabidopsis: *arf6-2* in Col-0	[38]	NASC: N24606
Arabidopsis: *UBI10::XVE>>amiR-MP* in Col-0	[8]	N/A
Arabidopsis: *PER15::H2B-3xm-Cherry* in *MYB84::NLS-3xGFP* in W131Y	This manuscript	N/A
Arabidopsis: *CASP1::shy2-2* in Col-0	[10]	N/A
Arabidopsis: *35S::TUA6-GFP* in Col-0	[21]	NASC: N6551
Arabidopsis: *PER15::slr-1-GR* in *MYB84::NLS-3xGFP* in W131Y	This manuscript	N/A
Arabidopsis: *XPP::shy2-2-GR* in *MYB84::NLS-3xGFP* in W131Y	This manuscript	N/A
Arabidopsis: *bp-9* in Col-0	[47]	N/A
Arabidopsis: *wox4-1* in Col-0	[42]	N/A
Arabidopsis: *WOX4::ER-YFP* in Col-0	[42]	N/A
Arabidopsis: *BP/KNAT1::NLS-3xm-Cherry* in *MYB84::NLS-3xGFP* in W131Y	This manuscript	N/A

(*Continued on next page*)

Continued

REAGENT or RESOURCE	SOURCE	IDENTIFIER
Arabidopsis: *XPP::m-Citrine-SYP122* in Col-0	[20]	N/A
Arabidopsis: *PER15::WOX4-GR* in W131Y	This manuscript	N/A
Arabidopsis: *PER15::BP-GR* in Col-0	This manuscript	N/A
Arabidopsis: *PXY::shy2-2-GR* in W131Y	This manuscript	N/A
Arabidopsis: *pxy-3* in Col-0	[20]	NASC: N9871
Arabidopsis: *PXY::ER-CFP* in Col-0	[48]	N/A
Arabidopsis: *mol1-1* in Col-0	[31]	N/A
Arabidopsis: *pMOL1::ER-YFP* in *PXY::ER-CFP*	[49]	N/A
Arabidopsis: *PXY::BP-GR* in W131Y	This manuscript	N/A
Arabidopsis: *35S::GR-MP* in Col-0	[14]	N/A
Arabidopsis: *gLBD16-SRDX* in Col-0	[50]	N/A
Arabidopsis: *rty1-1/+* in *DR5::GUS*	[22]	NASC: N16708
Arabidopsis: *DR5::GUS* in Col-0	[51]	from segregation of N16708
Oligonucleotides		
See Table S1	Sigma	N/A
Recombinant DNA		
PER15::slr-1-GR	This manuscript	See Data S1
XPP::shy2-2-GR	This manuscript	See Data S1
IAA28::NLS-3xm-Cherry	This manuscript	See Data S1
IAA14/SLR::NLS-3xm-Cherry	This manuscript	See Data S1
BP::NLS-3xm-Cherry	This manuscript	See Data S1
PER15::BP-GR	This manuscript	See Data S1
PER15::WOX4-GR	This manuscript	See Data S1
PER15::H2B-3xm-Cherry	This manuscript	See Data S1
PXY::shy2-2-GR	This manuscript	See Data S1
PXY::BP-GR	This manuscript	See Data S1
Software and Algorithms		
ZEN Black (Zen 2.3 SP1)	Zeiss	https://www.zeiss.de
Fiji	[52]	https://fiji.sc/
IBM SPSS Statistics version 24-25-26	IBM	https://www.ibm.com/products/spss-statistics
CFX Maestro	BIO-RAD	www.bio-rad.com

RESOURCE AVAILABILITY

Lead Contact

Further information and requests for resources should be directed to and will be fulfilled by the Lead Contact, Laura Ragni (laura.ragni@zmbp.uni-tuebingen.de).

Materials Availability

There are no restrictions to the availability of the newly generated resources.

Data and Code Availability

This study did not generate any unique code. This study did not produce any unique NGS sequencing/ protein structure/microarray data.

EXPERIMENTAL MODEL AND SUBJECT DETAILS

Arabidopsis thaliana transgenic and mutant lines were used to performed experiments. The ecotype and the background of each line/ mutant is specified in the Key Resources Table. GFP-based fluorescent reporters were crossed to the W131Y line to outline the cells and experiments were performed with F2 segregating and/or F3 homozygous populations. Plants were grown in continuous light condition *in vitro* on ½ MS plates supplemented with 1% sugar and 0.8% plant agar. For long auxin and NPA treatments, plants were grown on ½ MS and transferred after 7 days (unless it is specified otherwise in the text or figures) on ½ MS supplemented with 1μM NAA or 1μM IAA or 1μM 2,4D or 10μM NPA respectively. For β-Estradiol induction, plants were grown on ½ MS and transferred after 7 days on plates supplemented with 5μM β-Estradiol. For DEX induction, plants were grown on ½ MS and after 7days transferred (unless it is specified otherwise in the text or figures on plates supplemented with 10 μM DEX.

METHOD DETAILS

Molecular Cloning

All constructs have been obtained using the modular green gate technology [53]. Promoters were amplified from genomic DNA and the BP/KNAT1 coding sequence from root c-DNA with the primers listed in Data S1. If a BSAI site was present in the sequence, it was replaced as previously described in [54]. All modules and vectors used in this study are described in Data S1. The module assembly strategy is described in Data S1. All final plasmids were transformed into Agrobacterium tumefaciens GV3101. *Arabidopsis thaliana* plants were transformed via floral dipping. Homozygous T3 lines were used unless specified otherwise.

Histology and Fluorescent Stainings

Root samples for plastic embedding were taken 0.5mm from the root junction unless stated otherwise. Thin plastic cross-sections were obtained as described in [55], using Technovit 7100. 5-7 μm plastic sections were stained with 0.1% toluidine blue and imaged with a Zeiss Axio M2 imager microscope or a Zeiss Axiophot microscope. Fluorol yellow (FY) staining for suberin deposition was performed as described in [56] using Fluorol yellow. Propidium Iodide (PI) staining was achieved by directly mounting the root in a 10-20 μg/ml solution. GUS staining was performed as described in [6] using X-Glux. Roots were mounted in chloral hydrate solution (8:3:1; Chloral hydrate: Water: Glycerol).

Confocal Microscopy

Confocal images were acquired from whole-mount samples using a Zeiss LSM880 with the following settings. For Cyan fluorescent protein (CFP): excitation wavelength (ex.) 458 nm; emission (em.) 464–499 nm; For green fluorescent protein (GFP): ex. 488 nm; em 490–510 nm. For yellow fluorescent protein (YFP), mCitrine and Venus: ex. 514 nm; em. 520–540 nm. For mCherry, d-Tomato and PI: ex. 561 nm; em. 570–630 nm. For FY: ex. 488nm; em 490-540nm. For phellem autofluorescence: ex. 405 nm; em. 420–460 nm. 3D reconstructions, Orthogonal views of a Z stack and the ratio images of R2D2 were obtained using the ZEN Black software (Zen 2.3 SP1).

Periderm Quantification and Image Analyses

No statistical methods were used to predetermine sample size. The experiments were not randomized. Only few experiments were performed and analyzed blindly. Phellem length and Phellem ratio were measured as described in [6] using Fiji (https://fiji.sc/) [52]. At least 2-3 independent experiments were performed and the graphs of one representative experiment each are presented. The number of periderm layers was calculated as follow: the minimum and the maximum number of periderm layers per cross-section/sample was measured. For every genotype 9-20 cross-sections, coming from independent plants, were analyzed. According to the min and max number of layers, a sample was assigned to a certain class. For instance, if a sample has minimum 3 layers and maximum 4 layers, it was assigned to class 3-4. The frequency for each class was calculated and displayed as percentage. At least 2-3 independent experiments were performed and the graphs of one representative experiment is presented. The number of pericycle divisions upon auxin induction, was calculates using the *35S::TUA6-GFP* marker. Confocal Z stack images of two regions of the uppermost part of the root were acquired using the tile function (with 5% overlap). 8-9 roots per conditions were analyzed. The number of pericycle cells divisions per region of interest (ROI:(3x1 tiles: ≈600 μm) was quantified using the cell counter plugin of Fiji. The experiment was repeated twice and one representative is presented. The number of pericycle/periderm cells was quantified, measuring the number of pericycle/periderm cells in a cross-section using the cell counter plug in of FiJi for 10-12 roots.

Lateral Root Density

Lateral root density was measured counting the number of lateral root primordia present in 7-day-old roots and dividing it by the root length in cm or by counting the number of emerged lateral root in present in 12-day-old roots and dividing it by the root length in cm.

q-PCR

RNA was extracted from upper most 3cm of at least 30 roots for each genotype/treatment using the Universal RNA Purification Kit (Roboklon, E3598-02) according to the manufacturer protocol. C-DNA was synthetized using AMV Reverse Transcriptase Native (Roboklon, E1372-01) according to manufacturer protocol. qPCR was performed using MESA blue (Eurogentec, RT-SYS2X-03-+NRWOUB) in a CFX96 Real-Time System machine (BIO-RAD). Primers used for qPCR are listed in Table S1. The relative expression was calculated using *CFX Maestro software (*BIO-RAD) and the sample were normalized against EF1. qPCR experiments were repeated at least 3 times and one experiment is shown.

Gene List

The gene number and the full name of all genes mention in this study is presented in Data S1.

QUANTIFICATION AND STATISTICAL ANALYSES

We performed statistical analyses using IBM SPSS Statistics version 24-25-26 (IBM). The datasets were at first tested for homogeneity of variances using the Levene's Test. Then the significant differences between two datasets were calculated using a Welch's t test in case of a non-homogeneous variance or a Student's t test if the variance was homogeneous. The threshold for significance is indicated with P in the graphs. For multiple sample comparison, we calculated the significant differences between each dataset using One-way ANOVA with Tamhane's post hoc (equal variance not assumed) or a Bonferroni correction (equal variance assumed). The statistical analyses of the root length relative to phellem ratio and lateral root density measurement can be found in Data S2.